

Multi-objective optimization design of anti-roll torsion bar using improved beluga whale optimization algorithm

Yonghua Li and Zhe Chen

School of Locomotive and Rolling Stock Engineering, Dalian Jiaotong University, Dalian, China

Maorui Hou

Railway Science and Technology Research and Development Center, China Academy of Railway Sciences Corporation Limited, Beijing, China, and

Tao Guo

CRCC Tangshan Railway Vehicles Co Ltd., CRCC Tangshan Co Ltd, Tangshan, China

Abstract

Purpose – This study aims to reduce the redundant weight of the anti-roll torsion bar brought by the traditional empirical design and improving its strength and stiffness.

Design/methodology/approach – Based on the finite element approach coupled with the improved beluga whale optimization (IBWO) algorithm, a collaborative optimization method is suggested to optimize the design of the anti-roll torsion bar structure and weight. The dimensions and material properties of the torsion bar were defined as random variables, and the torsion bar's mass and strength were investigated using finite elements. Then, chaotic mapping and differential evolution (DE) operators are introduced to improve the beluga whale optimization (BWO) algorithm and run case studies.

Findings – The findings demonstrate that the IBWO has superior solution set distribution uniformity, convergence speed, solution correctness and stability than the BWO. The IBWO algorithm is used to optimize the anti-roll torsion bar design. The error between the optimization and finite element simulation results was less than 1%. The weight of the optimized anti-roll torsion bar was lessened by 4%, the maximum stress was reduced by 35% and the stiffness was increased by 1.9%.

Originality/value – The study provides a methodological reference for the simulation optimization process of the lateral anti-roll torsion bar.

Keywords Anti-roll torsion bar, Multi-objective optimization, IBWO, Chaotic mapping, Differential evolution
Paper type Research paper



1. Introduction

In order to ensure the comfort of passengers and the smoothness of vehicle operation, most of the rail vehicles use the softer two-system pendant suspension system, but the large flexibility of the two-system pendant suspension system also brings the problem of insufficient vehicle anti-roll stiffness. In order to solve the above problems, the addition of an anti-roll torsion bar system can be used.

As an important suspension component of a rail vehicle, the accurate calculation of the anti-roll stiffness value of the anti-roll torsion bar system is an important guarantee to make it meet the design requirements. In the traditional design process of anti-roll torsion bar, the main calculation method is the combination of finite element simulation calculation and theoretical calculation. However, the existing theoretical calculation method has the disadvantage of insufficient accuracy, and the design redundancy is large to ensure safety and increase the weight of anti-roll torsion bar (Zeng, Chi, & Dai, 2023).

At present, relevant scholars for railway vehicle anti-roll torsion bar stiffness theoretical calculation method to explore are in the initial stage, the proposed calculation method is not comprehensive enough to consider the factors, the results of the calculation and the actual value of the error is larger. Dong and Shang (2020) derived the stiffness equation of the anti-roll torsion bar in detail. In the optimization process, finite element method is utilized to calculate the stiffness and strength of the anti-rolling torsion bar under two loads, while topology optimization and parametric analysis are carried out for the torsion bar arm. The outcomes demonstrate that the mass of the optimized structure was decreased by 12.4% while maintaining the required stiffness and strength. The efficacy of combining finite element analysis (FEA) with topology-optimized design and dimensional-optimized design techniques was demonstrated. Shu and Liu (2017) established the rail vehicle anti-rolling torsion bar stiffness calculation model. Duan and Yuan (2019) propose a method for evaluating structures' static and fatigue strengths based on the theory of elasticity mechanics, which is simple and easy to parameterize. To satisfy the design requirements of the structure, Niu, Wang, Liao, Zhu, Zhang, and Keshtegar (2020) constructed a fatigue reliability analysis and optimal design framework of the bladed disk structure incorporating multivariate uncertainties based on the finite element method. The findings indicate that the optimization method based on the Kriging agent model is the best and significantly improves the reliability of the bladed disk structure.

The multi-objective optimization algorithm provides an effective means for the lightweight design of mechanical structures by considering the requirements and constraints of strength and stiffness while realizing the lightweighting of mechanical structures (Shanmugam & Sirisha, 2022, Babajamali *et al.*, 2022). Mi, Gu, Zhang, Liu, Zhang, and Nie (2016) proposed a kriging model-based collaborative optimization method to achieve frame lightweighting without the expense of fatigue life and strength. Li, Sheng, Zhi, and Li (2019) optimized the volume and stiffness of the anti-roll torsion bar using the Modified Non-dominated Sorting Genetic Algorithm (MNSGA)-III multi-objective algorithm. The optimized anti-roll torsion bar's stiffness rose by 3.3% while the volume was reduced by 1.6%, proving the effectiveness of the multi-objective optimization algorithm. Zhi, Wang, Chen, and Sheng (2022) constructed a multi-objective fuzzy optimization design model of the anti-roll torsion bar considering variable stiffness and strength reliability constraints. Through the example verification, the dependability of the anti-roll torsion bar is improved by 14% and the weight of the torsion bar is reduced by 0.6% during the life cycle. The effectiveness of the proposed method is verified. For the side-rolling torsion bar, Dong and Li (2015) offers a multi-response robust optimization design method based on a stochastic model. The results show that the optimized anti-roll bar has reduced weight, increased stiffness and fatigue strength while improving the anti-roll bar's anti-torsion capability. Zhang, Li, Bai, and Wang (2023) determined the input variables of the optimization model of the bogie frame structure through sensitivity analysis and carried out multi-objective optimization of the bogie frame using the improved Non-dominated Sorting Genetic Algorithm (NSGA)-II algorithm, and after

optimization, the maximum equivalent force of the bogie frame was reduced and its own weight was reduced, so as to achieve the lightweighting of the bogie frame.

Most researchers design anti-roll torsion bars with only FEA in mind or just use size-optimization algorithms. Zeng, Song, Li, Yan, and You (2021) optimized the turbine disk structure by intelligent optimization algorithm to decrease the mass of turbine disk. Zhang, Du, Mao, Meng, and Zhu (2022) suggested a tractor transmission case optimization method to achieve lightweight with the case meeting the strength and stiffness requirements. In 2022, Zhong, Li, and Meng (2022) introduced a meta-heuristic algorithm based on the behavior of the beluga whale, called the beluga whale optimization (BWO) algorithm. The results demonstrate that BWO performs well in single-objective optimization when compared to 15 other algorithms. In four engineering situations, BWO is adept at resolving complex engineering problems. However, the beluga optimization algorithm still suffers from problems such as uneven population distribution, poor spatial search ability and prematurely falling into local optimality. Chen, Zhang, and Wang (2023) address the shortcomings of the standard beluga optimization algorithm, such as low convergence accuracy and limited adaptive ability and adopt Fuch chaotic initialization to improve the traversability of the algorithm's initialized population, thus enhancing the algorithm's optimization searching accuracy and introduce the Fuch chaotic mapping in the development stage to coordinate the algorithm's global searching and local searching, which effectively improves the algorithm's adaptive ability. Chen, Zheng, Li, Zhang, and Zhu (2023) propose an update elite group mechanism for the standard Beluga Whale algorithm which has the defects of being prone to falling into local optimum and losing suboptimal solutions; secondly, in order to enhance the exploratory ability of the algorithm, a reverse learning strategy is added at the same time.

To address these problems, Logistic chaotic mapping, differential evolution (DE) strategy, crossover operation and Levy flight strategy are introduced to improve the uniformity and stability of the solution set distribution of the beluga optimization algorithm, as well as to enhance the global search and local utilization ability in this paper.

Taking the anti-rollover torsion bar as the research object, its working principle is briefly introduced and the strength of the torsion bar is analyzed by finite element method. An improved beluga whale optimization (IBWO) algorithm is proposed and the superiority and effectiveness of the algorithm is demonstrated through a case study. In order to test the feasibility and effectiveness of the proposed algorithm in solving the multi-objective optimization problem of anti-roll torsion bar, the multi-objective optimization algorithm is used to optimize the size of anti-roll torsion bar, so that the anti-roll torsion bar can realize the lightweight design under the demand of strength and stiffness, and the optimized torsion bar is simulated and verified. Through the combination of finite element simulation and multi-objective optimization algorithm, the optimal design size can be found to avoid the redundant design brought by the traditional design method.

2. Finite element analysis of anti-roll torsion bar

2.1 Calculation of anti-roll stiffness

The anti-roll torsion bar, as depicted in Figure 1, primarily consists of parts such as a torsion bar, torsion arms, connecting rods and support seats.

In Figure 1, B_e is the effective length, F is the connecting rod's axial force, θ is the side tilt the vehicle's body's angle, L is torsion arm's length, ζ is the vertical displacement of the rod and γ is the torsion angle of the torsion bar. The anti-roll stiffness k_t of the anti-roll torsion bar device is determined by dividing the torsional reaction value M of the torsion bar by the side tilt angle of the vehicle body.

One of the key performance indicators for the bogie, the anti-roll stiffness, is primarily influenced by the torsion bar's torsional rigidity. Thus, when other parameters are disregarded, the anti-roll stiffness can be described as follows:

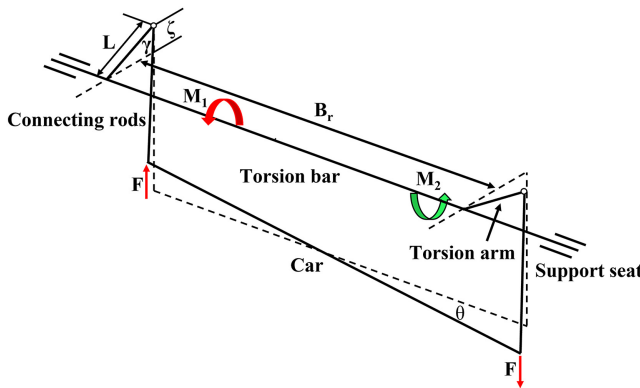


Figure 1. Working principle of anti-roll torsion bar device

Source(s): Authors' own work

$$k_t = \frac{B_r^2}{L^2} \cdot \sum_{i=1}^k G \cdot \frac{\pi \cdot D_i^4}{32L_i} \quad (1)$$

where L_i and D_i represent the length and diameter of each portion that falls within the torsion bar's range of torsional distortion.

2.2 Strength analysis of the torsion bar

The material properties of component of the anti-roll torsion bar are shown in Table 1.

According to the working principle of Figure 1, the finite element model is also set up as far as possible in the FEA in accordance with the boundary conditions of the real vehicle; as shown in Figure 2, fixed constraints are applied to the support seat and vertical loading is applied to the upper surfaces of the rubber nodes of the connecting rods at both ends, respectively. In accordance with the relevant technical standard CRH3-350-PS-021, the main tests for torsion bars are the static load conditions of the ultimate load and the fatigue load conditions.

Load case I: Maximum stress does not surpass the material's yield strength at the ultimate static load of 62kN.

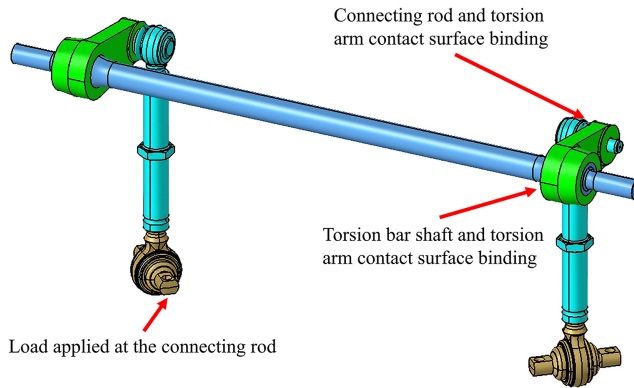
Load case II: Maximum stress does not surpass the material's yield strength under the 37kN fatigue dynamic load.

Figure 3 shows the anti-roll torsion bar's stress distribution as estimated by FEA. The torsion bar's maximal von Mises stress is located at the transition between the torsion bar and the torsion arm seat in load cases I (a) and II (b) because The transition is affected by a torque

Part name	Material	Young's modulus/ MPa	Density/ kg·m ⁻³	Poisson's ratio	σ_s /MPa	σ_b /MPa
Torsion bar	52CrMoV4	2.11×10^5	7830	0.30	1300	1450
Torsion arm	42CrMo	2.12×10^5	7850	0.28	650	930
Connecting rod	42CrMo	2.12×10^5	7850	0.28	650	930

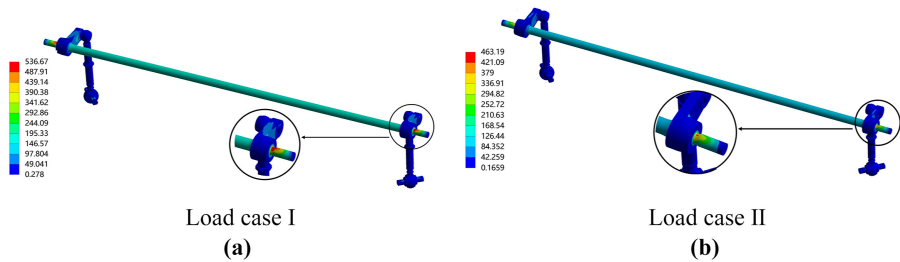
Source(s): Authors' own work

Table 1. Material of anti-roll torsion bar



Source(s): Authors' own work

Figure 2.
Boundary conditions of the anti-roll torsion bar



Source(s): Authors' own work

Figure 3.
FEA-derived stress distribution

and bending moment. The maximum equivalent stresses are 536.67 MPa and 463.19 MPa, which are less than the material's yield limit of 1300 MPa and fatigue limit of 745 MPa, respectively. Therefore, the torsion bar's static and fatigue strength complies with the design specifications.

3. Improved beluga whale optimization algorithm

3.1 Beluga whale optimization (BWO)

The BWO algorithm was inspired by the behavior of beluga whales, including swimming, feeding and whale falling. The BWO algorithm has an exploration phase, a development phase and a whale-falling phase. During the optimization process, the whale fall phase is implemented at the completion of each iteration of the exploration and mining phases. The steps of the original white whale optimization algorithm are as follows.

Step 1: Initialization

Determine the algorithm parameters, including the population size and the maximum number of iterations T_{max} . Randomly generate the initial positions of all belugas in the search space.

Step 2: Exploration and exploitation phase

Depending on the balancing factor B_f , each beluga chooses whether to join the exploration phase or the exploitation phase. If $B_f > 0.5$, the whale enters the exploration phase of the beluga is refreshed by [equation \(2\)](#).

$$\left\{ \begin{array}{l} X_{ij}^{T+1} = X_{i,p_j}^T + (X_{r,p_1}^T - X_{i,p_j}^T) \cdot (1 + r_1) \sin(2\pi r_2), j = \text{even} \\ X_{ij}^{T+1} = X_{i,p_j}^T + (X_{r,p_1}^T - X_{i,p_j}^T) \cdot (1 + r_1) \cos(2\pi r_2), j = \text{odd} \end{array} \right\} \quad (2)$$

where the current iteration, X_{ij}^{T+1} is the new location, p_j is a random number, X_{i,p_j}^T is the position of the i th beluga whale on p_j dimension, X_{i,p_j}^T and X_{r,p_1}^T are the current positions for i th and r th beluga whale (r is a randomly selected beluga whale), r_1 and r_2 are random number between (0,1). Two random numbers r_1 and r_2 are used to enhance the random operators in the exploration phase. If $B_f < 0.5$, then it enters the exploitation control phase, which is updated using equation (3). Then the fitness value of the new location is calculated and ranked to find the best result in the current iteration.

$$X_i^{T+1} = r_3 \cdot X_{best}^T - r_4 \cdot X_i^T + 2r_4 \cdot (1 - T/T_{max}) \cdot L_F \cdot (X_r^T - X_i^T) \quad (3)$$

where X_i^T and X_r^T are current position for the i th beluga whale and a random beluga whale, X_i^{T+1} is the new position of the i th beluga whale, X_{best}^T is the best position among beluga whales, r_3 and r_4 are random number (0,1). L_F is the Levy flight function, calculated as follows:

$$L_F = 0.05 \cdot \frac{u \cdot \sigma}{|v|^{1/\beta}} \quad (4)$$

$$\sigma = \left(\frac{\Gamma \cdot (1 + \beta) \cdot \sin(\pi\beta/2)}{\Gamma \cdot ((1 + \beta)/2) \cdot \beta \cdot 2^{(\beta-1)/2}} \right) \quad (5)$$

where u and v are random integers with normal distribution and β is 1.5.

Step 3: Whale fall phase

Some belugas could pass away and fall into the ocean, and the probability of the whale falling is calculated at each iteration W_f . Thus, the location of the belugas is updated according to equation (6).

$$X_i^{T+1} = r_5 \cdot X_i^T - r_6 \cdot X_r^T + r_7 \cdot X_{step} \quad (6)$$

where r_5 , r_6 and r_7 are random numbers between (0,1), X_{step} is the step size of whale fall established as:

$$X_{step} = (u_b - l_b) \cdot \exp(-2W_f \cdot n \cdot T/T_{max}) \quad (7)$$

The likelihood of a whale falling is estimated using this model as a linear function:

$$W_f = 0.1 - 0.05 \cdot T/T_{max} \quad (8)$$

The authors look forward to the development of the BWO multi-objective optimization algorithm. Insufficient population variety and inadequate spatial search capability are issues with the multi-objective white whale optimization algorithm that is prone to local optimum. These issues are addressed in this study. The introduction of logistic chaotic mapping and the difference variation operator enhances the algorithm's overall performance. Besides, in this paper, to expand the search step, the coefficient of 0.05 in equation (4) is modified to 1.

3.2 Logistic mapping

In order to improve population variety and provide early candidate solutions, chaotic mapping is applied. In addition to improving exploration capabilities, chaotic mappings can also assist optimization algorithms successfully avoid local optimum solutions (Ibrahim, Elaziz, & Lu, 2018; Wang, Li, Hu, & Yang, 2022; Zhang, Zhou *et al.*, 2022). Two popular mapping techniques for determining the starting points of optimization algorithms, Logistic and Tent mapping, are used in this paper to generate initial values. Logistic mapping can be described as equation (9):

$$x \cdot (k+1) = \mu \cdot x(k) \cdot (1 - x(k)) \quad (9)$$

where $x(k) \in (0, 1)$ and $3.5699 < \mu \leq 4$, the system is in chaos. When μ is close to 4, the chaotic sequence that is created is evenly spaced between 0 and 1, non-converging and non-periodic. Therefore, the control parameter μ should be set close to 4 (Zhang & Ding, 2021). Logistic mapping is employed to obtain the $x_{ij}(k+1)$ by equation (10).

$$x_{ij} \cdot (k+1) = 4 \cdot x_{ij}(k) \cdot (1 - x_{ij}(k)) \quad (10)$$

where, in accordance with equation, $x_{ij}(k+1)$ is converted from the original domain of [0,1] to a new x_{ij} according to equation (11), where ub and lb stand for, respectively, the upper bound and lower bound of x_{ij} .

$$x_{ij} = lb + x_{ij} \cdot (k+1) \cdot (ub - lb) \quad (11)$$

3.3 Differential evolution

DE strategies and crossover operations were introduced into BWO to generate new individuals. The differential variation strategy is a special variation strategy for the DE algorithm that involves scaling and combining the difference vectors of two randomly chosen individuals in the population to create a new individual. A crossover operation is carried out after mutation, and individuals are subjected to mutation with a specific probability to create a crossover population. The mutation and crossover operations are represented by equation (12) and equation (13), respectively.

$$V_{i,j} = x_{m1,j} + F(x_{m2,j} - x_{m3,j}), j=1, 2, \dots, D \quad (12)$$

$$u_{i,j} = \begin{cases} V_{i,j}, & \text{if } r \leq CR \text{ or } j = j_{rand} \\ x_{i,j}, & \text{else} \end{cases} \quad (13)$$

where $V_{i,j}$ stands for the mutant individual, $m1$, $m2$ and $m3$ for the randomly generated serial numbers for each individual. $x_{i,j}$ represents the variable in the original individual. F is the scaling factor and is taken as 0.8, CR is the crossover probability and is taken as 0.9, $r \in [0, 1]$, $j_{rand} \in [1, D]$ and integer number.

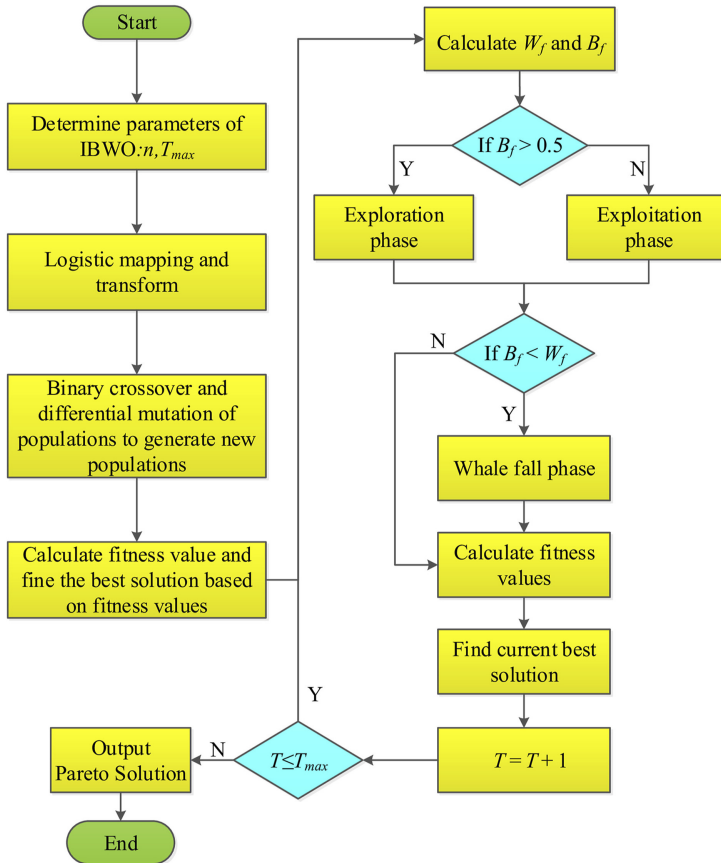
The DE factor has benefits such as an easy-to-use algorithm, stable search and a simple process. In this study, the DE algorithm is used to increase IBWO accuracy while also guaranteeing the algorithm's rapid convergence.

3.4 IBWO multi-objective optimization algorithm flowchart and case validation

The flowchart of the IBWO algorithm is illustrated in Figure 4.

Step 1: Input population size n and maximum number of iterations T_{max} .

Step 2: Logistic chaotic mapping is introduced and the population is chaotically initialized using Equation. (10).



Source(s): Authors' own work

Figure 4. Flowchart of the proposed IBWO

Step 3: Introduce DE strategies and crossover variants and use Equation (13) to generate new individuals.

Step 4: Determine the best individual and obtain the fitness value based on the objective function.

Step 5: Calculating B_f and W_f according to Equation (8). If the equilibrium factor $B_f > 0.5$, the updating mechanism enters the exploration phase and beluga whales are updated in terms of location through Equation (2). If $B_f < 0.5$, the update mechanism enters the exploitation phase, and the position is updated through Equation (3).

Step 6: Firstly, calculate the beluga whale fall probability W_f during the iteration process; secondly, perform the position update of beluga whale through Equation (6).

Step 7: the current iteration number T is greater than the maximum iteration number T_{max} , the algorithm stops, otherwise repeat from Step 5.

The four multi-objective optimization problems (MOP) test functions are solved using the proposed algorithm and the BWO algorithm. The calculation results are shown in Figure 5.

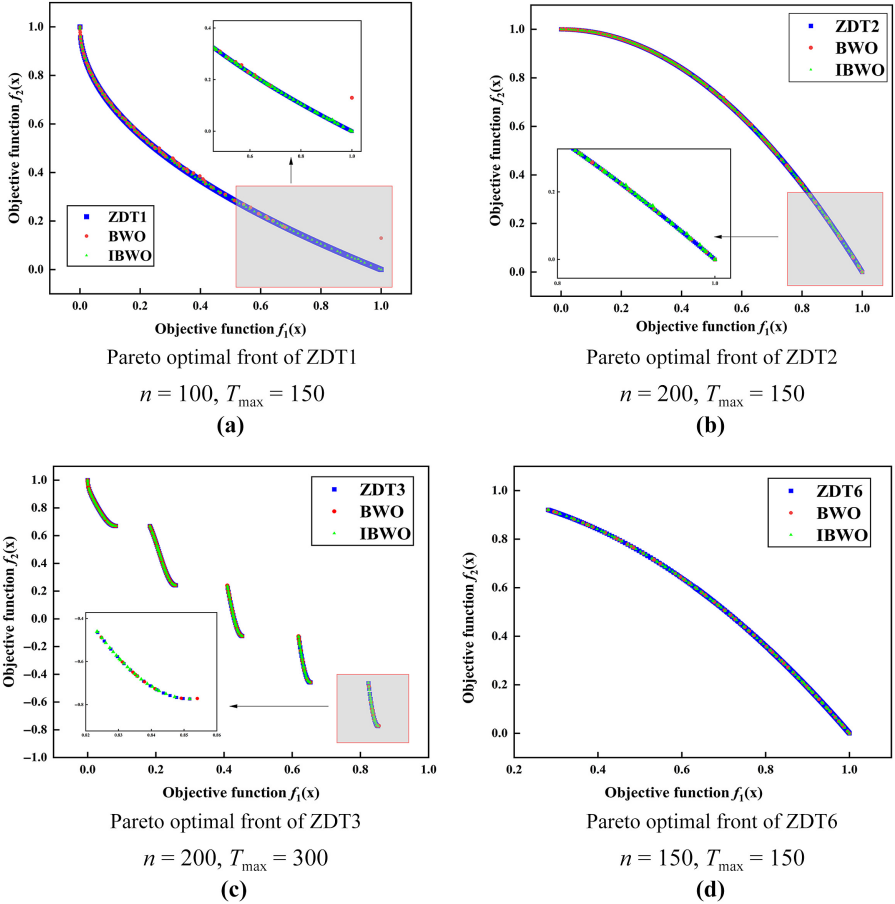


Figure 5.
Calculation results

Source(s): Authors' own work

The results in [Figure 5](#) demonstrate that both the algorithm used in this paper and the original algorithm produce better Pareto solution sets, but the distribution of individuals within some intervals is too concentrated in the original algorithm, and there are even no individuals in some regions. In addition, in order to quantitatively describe the computational performance of both algorithms, diversity criteria as shown in [equation \(14\)](#), which is commonly used in multi-objective algorithms for evaluation.

$$\Delta = \frac{h_f + h_l + \sum_{i=1}^{n-1} |h_i - \bar{h}|}{h_f + h_l + (n-1)\bar{h}} \quad (14)$$

where h_f and h_l are the Euclidean distances between the extreme and optimal solutions, respectively. h_i represents the distance between two adjacent points in the optimal solution, \bar{h} is the average value of h_i and n is the size of the solution set.

Each test function was run 30 times independently to obtain the mean and variance of the function are obtained in [Table 2](#).

Table 2 shows that the IBWO algorithm diversity means, and variance is smaller than BWO, and the variance is reduced by two orders of magnitude in the ZDT1 and ZDT2 test functions and by one order of magnitude in the ZDT3 and ZDT4 test functions. This demonstrates that the IBWO solution set's uniformity and extensiveness are superior to BWO.

4. IBWO-based torsion bar optimization and verification

4.1 Optimization model building

In this subsection, the material uncertainty is considered in the FEA and the material's coefficient of variation is set to 0.05. Figure 6 depicts the consideration of the four geometric dimensions of the torsion bar as design variables without changing the dimensions of the torsion arm.

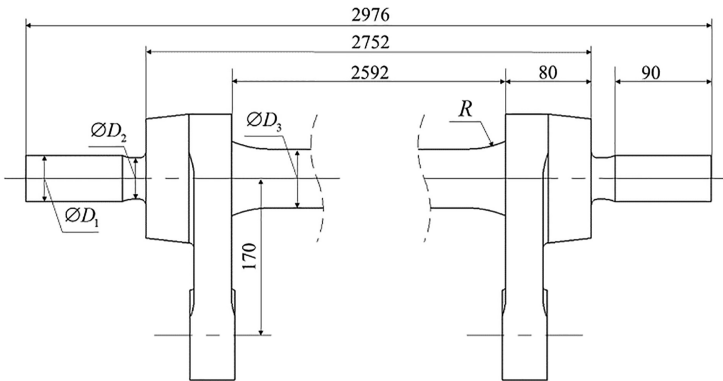
The relevant design codes determine the boundary conditions of the optimized design variables of the torsion bar, as shown in Table 3.

Random inputs were obtained using a Latin hypercube sampling of 30 groups, and the finite element outputs were used for quadratic polynomial response surface fitting. f_1 is a function of geometry and mass, and f_2 is an approximation function of geometry and maximum stress.

Test function	BWO		IBWO	
	Average value	Variance	Average value	Variance
ZDT1	0.863	0.0351	0.279	0.000679
ZDT2	0.911	0.0324	0.482	0.000918
ZDT3	1.031	0.00920	0.696	0.000607
ZDT6	0.949	0.00239	0.821	0.000592

Source(s): Authors' own work

Table 2. Comparison of average value and standard variance



Source(s): Authors' own work

Figure 6. Structural diagram of the torsion bar

Design variable (mm)	D1	D2	D3	R
Upper bound	45.15	40.43	57.54	94.5
Low bound	40.85	36.58	52	85.5

Source(s): Authors' own work

Table 3. Bounds of optimization variables

$$f_1(D_1, D_2, D_3, R) = 1694.12155 + 13.509 \times R + 13.916 \times D_1 - 19.155 \times D_2 - 50.321 \times D_3 - 0.037 \times R^2 + 0.289D_1^2 + 1.021 \times D_2^2 + 0.862 \times D_3^2 \quad (15)$$

$$f_2(D_1, D_2, D_3, R) = 87.598857 + 0.227 \times R + 2.906 \times D_1 - 5.37 \times D_2 + 0.732 \times D_3 - 0.0013 \times R^2 - 0.042 \times D_1^2 + 0.218 \times D_2^2 + 0.04 \times D_3^2 + 0.008 \times R \times D_1 - 0.017 \times R \times D_2 + 0.006 \times R \times D_3 - 0.051 \times D_1 \times D_2 - 0.01 \times D_1 \times D_3 + 0.008 \times D_2 \times D_3 \quad (16)$$

The evaluation index complex correlation coefficient r^2 test can be used to determine how well the response surface function fits the response value, and its expression is as [equation \(17\)](#), where Y_i is the calculated value of the response surface model, y_i is the calculated value of ANSYS and \bar{Y} is the average value of each Y_i .

$$r^2 = 1 - \frac{\sum_{i=1}^m (Y_i - y_i)^2}{\sum_{i=1}^m (Y_i - \bar{Y})^2} \quad (17)$$

The equation $r_1^2 = 1$ and $r_2^2 = 0.972$, shows that the response surface model of mass and maximum stress fits well and can reflect the relationship with the design variables.

4.2 Optimization process and results

In the case of satisfying the performance requirements such as strength and stiffness, the structure is optimized to realize the lightweight of the anti-rolling torsion bar. The stiffness of the anti-rolling torsion bar is $1.58 \text{ MN} \cdot \text{m/rad}$ calculated from [equation \(1\)](#), and the permissible condition of stiffness is determined by the design specification as $1.58 \pm 10\% \text{ MN} \cdot \text{m/rad}$. The stiffness is selected as the constraint, and the objective function is the minimum value of the torsion bar mass and the maximum stress. According to the above analysis, the mathematical model of torsion bar structure optimization is established as shown in [equation \(18\)](#).

$$\min f_1(D_1, D_2, D_3, R), f_2(D_1, D_2, D_3, R)$$

$$\text{s.t.} \left\{ \begin{array}{l} 1.42 \leq k_t \leq 1.73 \\ 40.85 \leq D_1 \leq 45.15 \\ 36.58 \leq D_2 \leq 40.43 \\ 52 \leq D_3 \leq 57.54 \\ 85.5 \leq R \leq 94.5 \end{array} \right. \quad (18)$$

The population size is set to 100, and the number of evolutionary generations is set to 300, taking into account the complexity of the actual situation. Figure 7 displays the obtained Pareto solution set.

Each point in the figure represents a set of optimal solutions, and the solutions are not dominated by each other. Due to the conflict between the objectives, the maximum stress of the structure decreases with increasing mass, and the designer can choose the corresponding solution according to the difference in focus. Optimization algorithm is used to find the optimal size of the anti-roll torsion bar, test 30 times, record the optimal result of each time and take the average at last. The optimal solution chosen in this paper is shown in Table 4.

4.3 Simulation analysis verification

The optimized design results are used to update the lateral roll resistance torsion bar model for static simulation verification, and the optimized stresses are shown in Figure 8.

The accuracy of the algorithm was verified by comparing the finite element calculation results with the extreme results of the optimization algorithm. The anti-roll torsion bar mass, maximum stress and anti-roll stiffness after optimization using the algorithm in this paper are depicted in Table 5. It is evident that, after optimization, the mass of the anti-roll torsion bar is decreased by 4%, the max stress under normal operating conditions is decreased by 35%, the max stress under extreme operating conditions is reduced by 8% and the stiffness of the anti-roll torsion bar is increased by 1.9%. The effectiveness and superiority of the algorithm in this paper are verified.

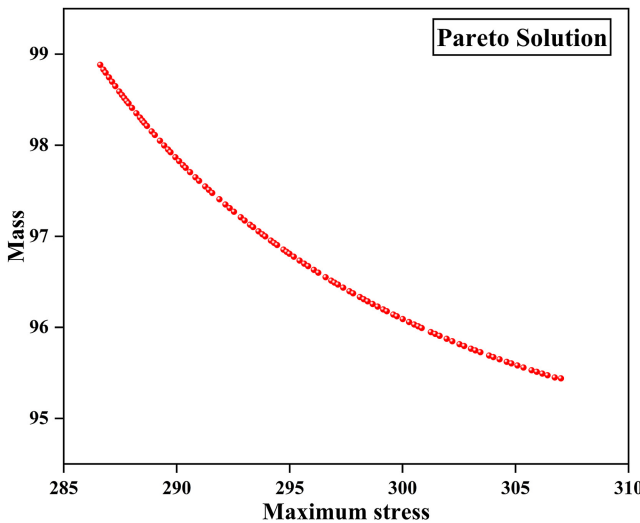


Figure 7. Pareto solution

Source(s): Authors' own work

Variables	D_1 /mm	D_2 /mm	D_3 /mm	R /mm	Mass (kg)	Stress (MPa)
Initial	43	38.5	54.8	90	100.8	463.19
Optimized	42	39.6	52.4	88.7	96.55	295.49

Source(s): Authors' own work

Table 4. Comparison of design variables before and after optimization

5. Conclusions

- (1) Combining the working principle and structural characteristics of the anti-roll torsion bar, analyzing its force, using finite element simulation combined with the white whale multi-objective optimization algorithm, static simulation to analyze the strength and stiffness performance of the anti-roll torsion bar. Moby Dick multi-objective optimization algorithm searches for the optimal size of the anti-roll torsion bar, avoiding the redundant mass in the traditional design and realizing the lightweight design.
- (2) An IBWO algorithm is proposed, and the BWO algorithm’s population variety is increased with the introduction of a logistic chaotic mapping approach. In addition, the introduction of a differential variance strategy improves the global search capability of the BWO algorithm. The test results of the algorithm show that the mean diversity values of the IBWO algorithm are 0.279, 0.482, 0.696 and 0.821 for ZDT1, ZDT2, ZDT3 and ZDT6 test functions, respectively, and the variances are 0.000679, 0.000918, 0.000607 and 0.000592, which are better than those of BWO at 0.863, 0.911, 1.031, 0.949 and 0.0351, 0.0324, 0.0092, 0.00239, respectively. It proves that the uniformity and extensiveness of the distribution of the solution set are better, which verifies the effectiveness of the proposed algorithm.
- (3) With the torsion bar mass and max stress as the optimization objective, the stiffness of the torsion bar against lateral roll is taken as the constraint, and the partial size of the torsion bar is taken as the design variable. The torsion bar size optimization is carried out based on the IBWO algorithm. After optimization, the mass of the anti-rolling torsion bar is 96.55kg, the maximum stress under 37kN load is 296.57MPa, the max stress under 67kN load is 496.96MPa and the anti-rolling stiffness is 1.61MN · m/rad. Better than 100.8kg, 463.17MPa, 536.67MPa and 1.58 MN · m/rad before optimization. The purpose of lightweighting is achieved while meeting the strength and stiffness requirements. The effectiveness of the simulation design technique integrating dimensional optimization design and finite element strength analysis is confirmed.

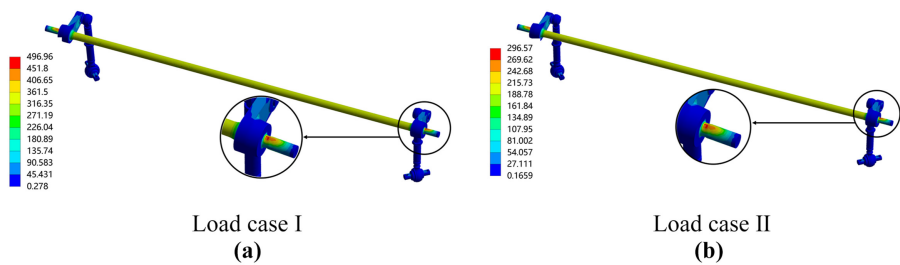


Figure 8. Maximum stress distribution after optimization

Source(s): Authors’ own work

Table 5. Comparison of the plan before and after optimization

Scheme	Mass (kg)	Maximum stress (MPa)	Anti-rolling stiffness (MN · m/rad)
		Load case I/Load case II	

Before optimization	100.8	536.67/463.17	1.58
After optimization	96.55	496.96/296.57	1.61

Source(s): Authors’ own work

In future research, the use of dynamics simulation to simulate the anti-roll torsion bar is more appropriate to the actual situation, but also other indicators such as stability as the constraints of multi-objective optimization, to further optimize the anti-roll torsion bar structure under the premise of guaranteeing safety, to achieve the design of lightweight, the future of the high-speed train system may be integrated into the intelligent and automated control technology. The anti-roll torsion bar system can be integrated with other intelligent sensors and control systems to realize automatic adjustment and control, in order to adapt to different operating conditions and provide a higher level of driving stability and safety.

References

- Babajamali, Z., Khabaz, M. K., Aghadavoudi, F., Farhatnia, F., Eftekhari, S. A., & Toghraie, D. (2022). Pareto multi-objective optimization of tandem cold rolling settings for reductions and inter stand tensions using NSGA-II. *ISA Transactions*, 130, 399–408.
- Chen, X. Y., Zhang, M. J., & Wang, D. G. (2023). Improved beluga whale optimization algorithms based on Fuch mapping and applications. *Computer Engineering and Science*. Available from: <http://kns.cnki.net/kcms/detail/43.1258.TP.20231024.1408.002.html>
- Chen, Y. J., Zheng, J. L., Li, Z. Q., Zhang, J. B., & Zhu, X. H. (2023). Improved beluga whale optimization for RFID network planning. *Computer Science*. Available from: <http://kns.cnki.net/kcms/detail/50.1075.TP.20230925.1926.192.html>
- Dong, S. D. and Li, Y. H. (2015). Multi-response robust optimization of anti-rolling torsion bar based on the stochastic model. *Journal of Railway Science and Engineering*, 12(4), 900–904.
- Dong, Y. H. and Shang, Y. J. (2020). Analysis of characteristics and structure optimization of anti-rolling torsion bar. In Tan, J. (Ed.), *Advances in mechanical design* (pp. 139-150), Springer Nature Singapore, ICMD 2019, *MMS* 77. doi: [10.1007/978-981-32-9941-2_12](https://doi.org/10.1007/978-981-32-9941-2_12).
- Duan, J. L. and Yuan, W. H. (2019). Project method of stiffness and strength analysis about anti-rolling torsion bar system of rail vehicle bogie. *Modern Manufacturing Engineering*, 7, 49–54.
- Ibrahim, R. A., Elaziz, M. A., & Lu, S. (2018). Chaotic opposition-based Grey-wolf optimization algorithm based on differential evolution and disruption operator for global optimization. *Expert Systems with Applications*, 108, 1–27.
- Li, Y. H., Sheng, Z. Q., Zhi, P. P., & Li, D. M. (2019). Multi-objective optimization design of anti-rolling torsion bar based on modified NSGA-III algorithm. *International Journal of Structural Integrity*, 12, 17–30.
- Niu, X. P., Wang, R. Z., Liao, D., Zhu, S. P., Zhang, X. C., & Keshtegar, B. (2020). Probabilistic modeling of uncertainties in fatigue reliability analysis of turbine bladed disks. *International Journal of Fatigue*, 142, 1–11. doi:[10.1016/j.ijfatigue.2020.105912](https://doi.org/10.1016/j.ijfatigue.2020.105912).
- Mi, C. J., Gu, Z. Q., Zhang, Y., Liu, S., Zhang, S., & Nie, D. Z. (2016). Frame weight and anti-fatigue Co-optimization of a mining dump truck based on kriging approximation model. *Engineering Failure Analysis*, 66, 99–109.
- Shanmugam, M., & Sirisha, M. L. (2022). Multi-objective optimization of parallel microchannel heat sink with inlet/outlet U, I, Z type manifold configuration by RSM and NSGA-II. *International Journal of Heat and Mass Transfer*, 201, 1–11. doi:[10.1016/j.ijheatmasstransfer.2022.123641](https://doi.org/10.1016/j.ijheatmasstransfer.2022.123641).
- Shu, B. and Liu, W. S. (2017). Analysis and calculation of bending bar integral stiffness for railway vehicles. *Railway Locomotive and Car*, 37, 47–49.
- Wang, J., Li, Y., Hu, G., & Yang, M. S. (2022). An enhanced artificial hummingbird algorithm and its application in truss topology engineering optimization. *Advanced Engineering Informatics*, 54, 1–50. doi:[10.1016/j.aei.2022.101761](https://doi.org/10.1016/j.aei.2022.101761).
- Zeng, N. Y., Song, D. D., Li, H., Yan, C., & You, Y. C. (2021). Improved whale optimization algorithm and turbine disk structure optimization. *Journal of Mechanical Engineering*, 57(4), 254–265.

-
- Zeng, P. C., Chi, M. R., & Dai, L. C. (2023). Research and verification of an antiroll stiffness optimal calculation method for railway vehicle antiroll torsion bar. *Journal of Mechanical Engineering*, *59*(16), 353–360.
- Zhang, C. L., & Ding, S. F. (2021). A stochastic configuration network based on chaotic sparrow search algorithm. *Knowledge-Based Systems*, *220*, 1–20. doi:[10.1016/j.knosys.2021.106924](https://doi.org/10.1016/j.knosys.2021.106924).
- Zhang, Y. A., Du, Y. F., Mao, E. R., Meng, Q. F., & Zhu, Z. X. (2022). Multi-objective optimization of high-horsepower tractor gear box based on improved NSGA-II. *Transactions of the Chinese Society for Agricultural Machinery*, *53*(s2), 310–319.
- Zhang, X. Y., Zhou, K. Q., Li, P. C., Xiang, Y. H., Zain, A. M., & Sarkheyli-Hägele, A. (2022). An improved chaos sparrow search optimization algorithm using adaptive weight modification and hybrid strategies. *IEEE Access*, *10*, 96159–96179.
- Zhang, D. X., Li, Y. H., Bai, X., & Wang, Y. F. (2023). Multi-objective optimization of bogie frame based on RBF-CLNSGA- II algorithm. *Journal of Railway Science and Engineering*. doi: [10.19713/j.cnki.43-1423/tu.T20230030](https://doi.org/10.19713/j.cnki.43-1423/tu.T20230030).
- Zhi, P. P., Wang, Z. L., Chen, B. Z., & Sheng, Z. Q. (2022). Time-variant reliability-based multi-objective fuzzy design optimization for anti-roll torsion bar of EMU. *Computer Modeling in Engineering and Sciences*, *131*, 1001–1022.
- Zhong, C. T., Li, G., & Meng, Z. (2022). Beluga whale optimization: A novel nature-inspired metaheuristic algorithm. *Knowledge-Based Systems*, *251*, 1–23. doi:[10.1016/j.knosys.2022.109215](https://doi.org/10.1016/j.knosys.2022.109215).

Corresponding author

Yonghua Li can be contacted at: yonghuali@163.com